Available online at www.eccomasproceedia.org
Eccomas Proceedia COMPDYN (2023) 528-543

ECCOMAS
Proceedia

COMPDYN 2023
9th ECCOMAS Thematic Conference on
Computational Methods in Structural Dynamics and Earthquake Engineering
M. Papadrakakis, M. Fragiadakis (eds.)
Athens, Greece, 12-14 June 2023

EXPERIMENTAL AND NUMERICAL INVESTIGATION OF THE SEISMIC RESPONSE OF CONFINED MASONRY WALLS

Nemanja Krtinić[1*], Matija Gams[1], Marko Marinković[2]

[1] University of Ljubljana, Faculty of Civil and Geodetic Engineering
Jamova cesta 2, 1000 Ljubljana, Slovenia
nemanja.krtinic@fgg.uni-lj.si, matija.gams@fgg.uni-lj.si

[2] University of Belgrade, Faculty of Civil Engineering
Bulevar kralja Aleksandra 73, 11000 Belgrade, Serbia
mmarinkovic@grf.bg.ac.rs

Abstract

Confined masonry (CM) is one of the most popular and affordable earthquake-resistant construction technology for masonry structures. The reinforced concrete (RC) tie-columns in such construction play a crucial role in improving seismic response. However, their interaction with the masonry warrants a review due to recent changes in masonry construction, which are typical for Southeastern Europe. The modern masonry walls built from clay units are thick to achieve thermal efficiency. The tie-columns size has also increased, but they are narrower than the masonry. A part of masonry thus protrudes from the area confined by tie columns, which can lead to stress concentrations and early onset of damage of the protruding masonry, as was observed in recent tests on such masonry. This paper numerically analyzes this problem using a detailed three-dimensional (3D) finite element (FE) model that can capture this effect. The numerical model was developed in ABAQUS, and uses Concrete Damage Plasticity (CDP) material model to model the brittle response of clay blocks. All input data for the numerical model were obtained by dedicated tests. The results are compared to tests of walls in terms of damage propagation, strength and deformation response and show that damage to the protruding masonry can be successfully modelled. The results show a good alignment with the experiments and can be used for detailed modelling of seismic response of CM masonry structures and further research.

Keywords: Confined masonry, Cyclic shear-compression test, Numerical modelling, Concrete Damage Plasticity (CDP).

ISSN:2623-3347
Peer-review under responsibility of the organizing committee of COMPDYN 2023.
doi: 10.7712/120123.10418.20831

1 INTRODUCTION

Confined masonry (CM) is considered one of the most popular construction systems for low- to mid-rise masonry buildings in earthquake-prone regions. Over the last 100 years, confined masonry (CM) construction has emerged as a building technology that offers an appealing alternative to both unreinforced masonry (URM) and masonry infilled reinforced concrete (RC) frames by involving the elements of both structural systems [1]. Given that the same materials are used to construct CM and RC buildings with masonry infills, CM buildings require significantly less advanced construction skills and equipment [2]. This automatically makes them a viable alternative to mid-rise RC frames with masonry infill. In the last century, confined masonry buildings have withstood the effects of major earthquakes around the world without collapse and especially performed very well in the 2010 Chile earthquake, which caused substantial damage to unreinforced masonry and RC buildings [3, 4]. It should also be emphasised that properly constructed confined masonry buildings have demonstrated good seismic performance compared to URM buildings in the recent Petrinja, Croatia M 6.4 earthquake [5].

Since CM walls are used mostly in low-rise buildings, damage in CM buildings during previous earthquakes is usually associated with damage at the first storey and occurs through two main failure modes related to shear and flexure [1, 2, 6, 7]. Due to their relatively low H/L ratio (less than 1.5), these walls are more likely to show shear-dominant behaviour when subjected to lateral load during an earthquake. Shear behaviour can lead to brittle failure and is characterized by the propagation of diagonal cracks from the centre of the masonry wall towards the ends of the tie-columns, damaging the tie-columns and shearing them off.

Load-bearing masonry walls in CM buildings are confined by small-sized RC columns and beams known as tie-columns and tie-beams, respectively. These elements prevent brittle seismic response of masonry walls, increase structure's ductility and protect walls from complete disintegration even in major earthquakes. Even if masonry walls suffer severe damage during an earthquake, tie-columns continue to resist a major portion of gravity load. Toothed interfaces (Wall-to-Tie-column) are also used to improve the seismic performance and post-peak behaviour of confined masonry walls, as reported in [1, 8].

In recent years, the brick industry has invested heavily into developing new products, especially modern masonry blocks. The cavities of modern blocks are filled with thermal insulation, which makes these blocks quite thick, usually thicker than the RC tie-columns. Experimental tests on two modern CM walls (which will be discussed in the next chapter) showed that the difference in wall thickness and RC tie-columns could lead to stress concentration and early onset of damage to protruding masonry.

Considering that most of the research related to CM walls is based on experimental testing, the numerical modelling and analysis of these walls seem a challenging task. Available numerical approaches for modelling CM walls based on the Finite Element Method (FEM) can be classified into micro and macro levels. Micro models are mainly used for parametric studies to investigate the influence of key design parameters on the seismic response of CM walls, i.e. tie-column size and reinforcement, wall aspect ratio, FE mesh, concrete to masonry interface, and axial stress level on the seismic behavior of CM walls [9-12].

According to Lourenco [13], the micro-model of masonry can be performed as detailed micro-modelling or simplified micro-modelling, depending on how the mortar in joints are modelled. In the simplified micro-modelling approach, which has been used in this study, mortar joints are not modelled as continuum elements. Instead, the joints are modelled by zero-thickness interfaces, which model the interaction between units and between units and the RC confining elements.

Hollow clay blocks were modelled in two ways, resulting in two 3D FE models. In the first numerical model, masonry units are modelled as solid elements without holes, and the effect of holes is taken into account by appropriately modifying material charateristics. The masonry units in the second numerical model are modelled as solid elements with holes identical to the ones in blocks used in the experiment.

The main objective of this paper is to develop a reliable three-dimensional (3D) FE model that can capture and successfully describe the effect of partial confinement, and interaction between masonry and RC tie-columns. 3D micro modelling was perfomred in the commercial software package Abaqus [14].

In this paper results of two experimental cyclic shear tests carried out on two full-scale modern confined masonry walls are presented. The two 3D FE models, results of the numerical analyses carried out in Abaqus [14], as well a comparison of experimental and numerical results in terms of damage, capacity curve and shear-off effect are given in chapter 3, followed by conclusions.

2 EXPERIMENTAL TESTS

In order to evaluate the seismic behaviour of CM walls in terms of damage evolution, capacity and ductility, cyclic shear compression tests on two full-scale modern CM walls (labelled W7 and W8) were conducted [15]. The gravity forces on the wall were simulated by additional vertical forces. The seismic (earthquake) loads were imposed on the wall in the form of prescribed displacements, which act cyclically in the positive and negative directions (three times) and with increasing amplitude until collapse. The walls were tested under so called fixed-fixed boundary conditions, in which there is no rotation at the top, and the vertical force is constant throughout the test. The detailed dimensions of the tested full-scale modern CM walls are given in Figure 1.

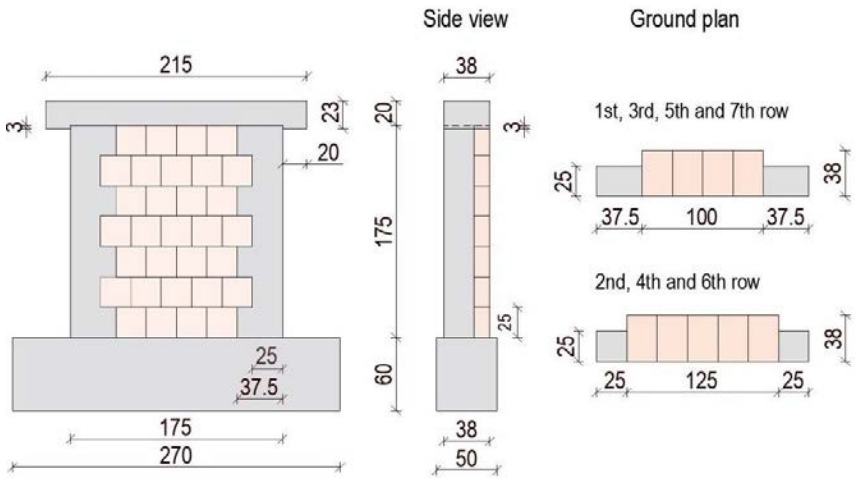

Figure 1: Dimensions of the tested walls (dimensions in cm).

2.1 Test specimens

The test specimens (W7 and W8) were built on RC foundations for easier transport and later fixing to the laboratory floor. They were constructed from hollow clay masonry blocks (dimensions of the unit are 250 x 249 x 380 mm) and polyurethane (PU) glue instead of thin-bed mortar. First, a layer of general-purpose mortar of about 1-2 cm thickness was laid on the RC foundation (bottom beam). The purpose of this mortar layer is to provide a level surface for the construction of the wall. The wall above was built using PU glue, which was applied

to the bed joints in four strips. At the time of application, the glue is in the form of foam but loses its volume after a short while. The final thickness of the bed joints is negligible (less than 1 mm). The PU glue is only applied to bed joints, since head joints were unfilled and inter locked with the tongue and groove type of contact. Perfect overlapping of units was used (overlap equals 0.5 length of the unit). A RC bond beams was constructed on top of the walls for the distribution of vertical and horizontal forces.

The dimensions of the tie-columns were 25 x 25 cm, which is larger than the minimum of 15 cm required by Eurocode 8. Minimal longitudinal reinforcement according to Eurocode 8 (1 % of cross-section area) was used, which amounted to 4 x Ø 14 mm rebars. Shear reinforcement was Ø 8 mm stirrups spaced at about 20 cm. Stell grade was B 500.

2.2 Test setup and experimental results

The test setup of the full-scale specimens (W7 and W8) consists of a strong laboratory floor, strong steel beam placed on the top of the tested walls for transfer the horizontal and vertical load to the CM wall, and hydraulic actuators. Vertical load is applied using two hydraulic actuators with servo control at the sides of the beam. These actuators are anchored to the laboratory floor via steel tie rods. Horizontal load is applied with a servo-controlled hydraulic actuator.

The horizontal movement of the bond beam is measured by an optical Digital Image Correlation (DIC) system. This system is also used for measuring the displacements and strains over the entire surface of a wall, including the foundation. The displacement field is measured only on one side of the wall, and there the wall is painted with contrasting random pattern. On the other side the wall is painted white to facilitate visual observation of the damage and cracks.

Based on experimentaly observed hysteretic curve, its envelope and observations during the test, three limit states were defined for each of the walls: Damage LS, Maximum resistance LS and Near collapse LS. For each of the limit states, the strain fields (in terms of major strains) on the surface of the walls were measured using an optical DIC system of the wall. The major strain fields of tested confined wall W8 at all three aforementioned limit states are shown in Figure 2. In the next subsection, the measured strain fields will be compared with numerical simulations in Abaqus [14].

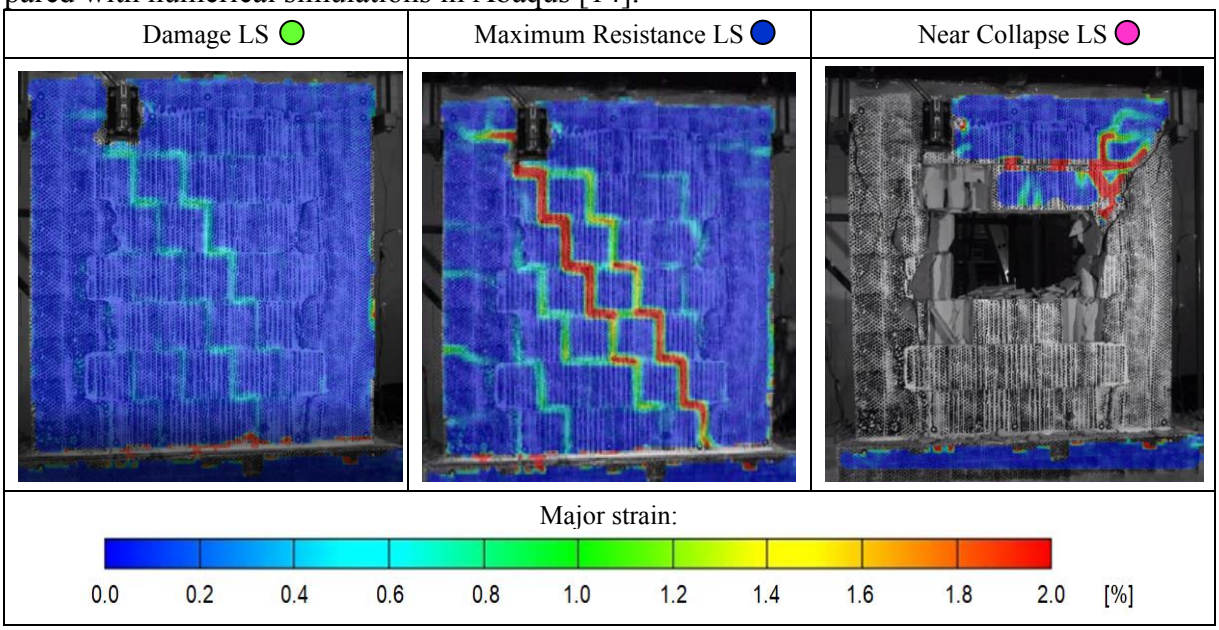

Figure 2: Limit states of the tested specimen W8 (MS = major strains).

Figure 3 shows the envelope curves for both walls that were used to compare with the results obtained from the numerical calculations. Limit states are denoted on the figure by differently colored circles (green circle-Damage LS, blue circle-Maximum Resistance LS and magenta circle-Near Collapse LS).

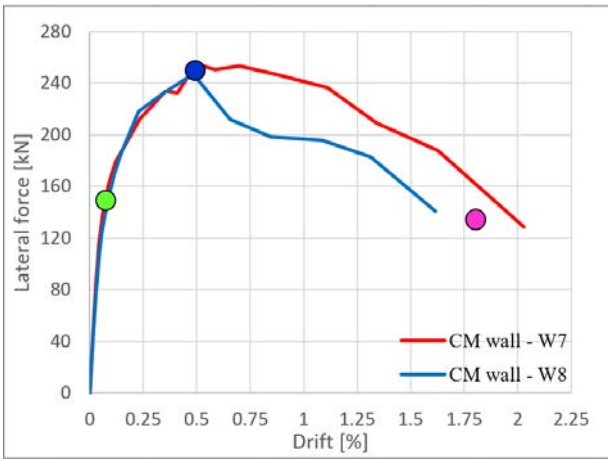

Figure 3: Experimental envelope curves of the tested confined masonry (CM) walls with highlighted limit states (Damege LS, Maximum resistance LS and Near collapse LS).

An interesting phenomenon was observed during the experimental tests. The protruding part of masonry, which was not confined by the tie-columns, developed damage rather early and started to sheared off (see Figure 4). The first indications of the this were observed at a drift of about 0.35 %.

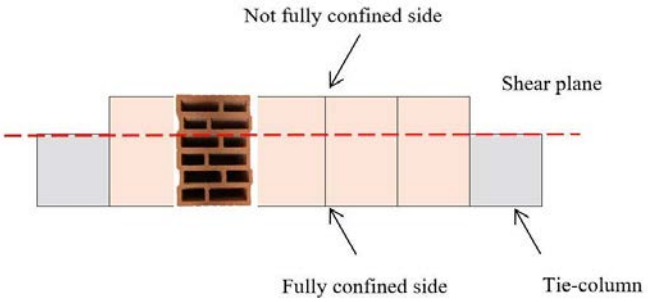

Figure 4: Different conditions on different sides of confined masonry walls and the shear plane.

This affects the local damage evolution, as the not fully confined side begins to crack and damage along a shear plane, as shown in Figure 4. At the maximum resistance of the walls of about 253 kN, which was reached at a drift of about 0.5 %, the protruding parts of the units were already significantly damaged (Figure 5a). Protruding parts completely sheared off at a drift of 1.3 % and dropped to the floor (Figure 5b).

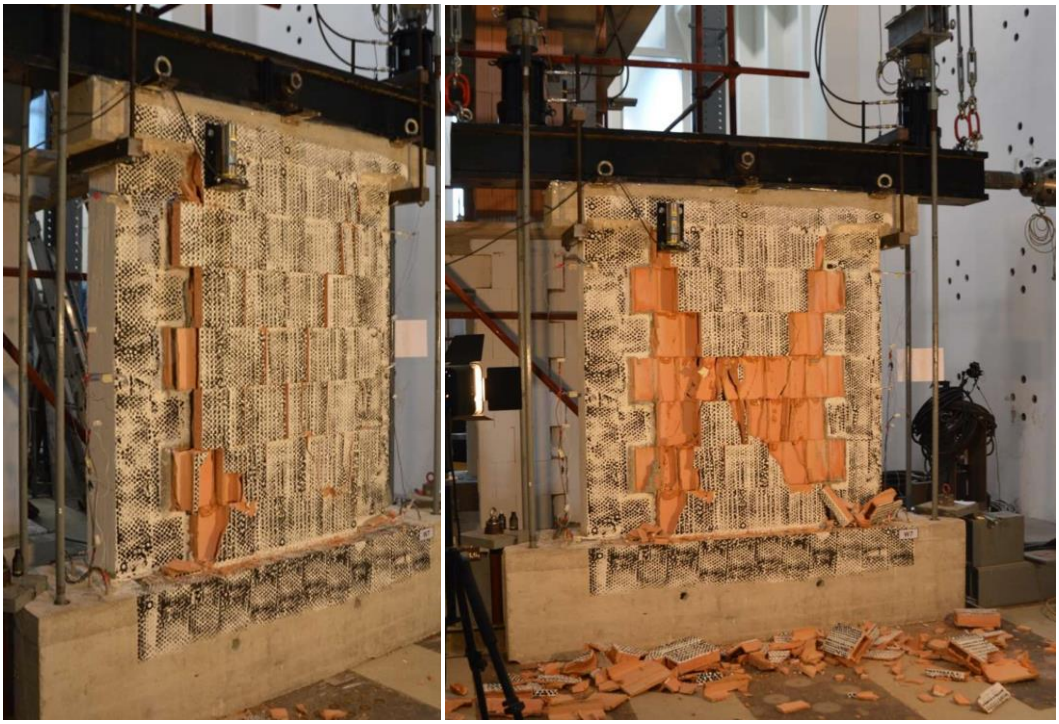

Figure 5: Shear-off effect of unconfined parts of masonry units a) at 0.5% drift (left) and b) at 1.3 % drift (right).

3 NUMERICAL SIMULATIONS OF CONFINED MASONRY WALLS

In order to study the response of CM walls under lateral loads, a three-dimensional (3D) FE model was developed. The model was designed so that it can also simulate the shearing off of the protruding masonry.

As mentioned, the numerical simulations were peformed in two steps, using progressively more detailed models. In the first numerical model the masonry blocks were modelled as solid elements, whereas in the second model, the units were modelled according to their actual geometry (with webs, shells and holes).

The material models (for concrete, masonry and steel reinforcement), loads and boundary conditions and interface are explained in the following. Finally, the simulations are compared to the experiments.

3.1 Description of the numerical models

Tie-columns, tie-beam and masonry units were modelled as three-dimensional continuum elements with 8 nodes with reduced integration (C3D8R). According to the recommendations of Abaqus [16], C3D8R elements are considered the most suitable elements for the explicit dynamic analysis used in these numerical simulations. The longitudinal reinforcement bars and stirrups have been modelled as wire 3D-truss elements with two nodes (T3D2). In order to achieve the interaction between different components of the wall (concrete and reinforcement), it was necessary to connect these elements. Thus, rebars were embedded in the surrounding concrete using the "Embedded Constraint" available in Abaqus [16]. This option allows the displacements of the reinforcement and concrete nodes to be equal. In order to simulate the boundary conditions in the experiment, a fixed boundary condition (BC) is assigned to the bottom surface of the bottom beam.

The confined masonry (CM) wall is modelled using the actual geometry of full-scale specimens (see Figure 1). The exception is the foundation, which is modelled as a discrete rigid

plate in order to reduce the computational costs, and it was connected with the tie-columns of by a "tie constraint". The longitudinal bars and stirrups are modelled as separate parts taking into account their actual length and exact position in masonry assembly. The geometry of the numerical model is shown in Figure 6.

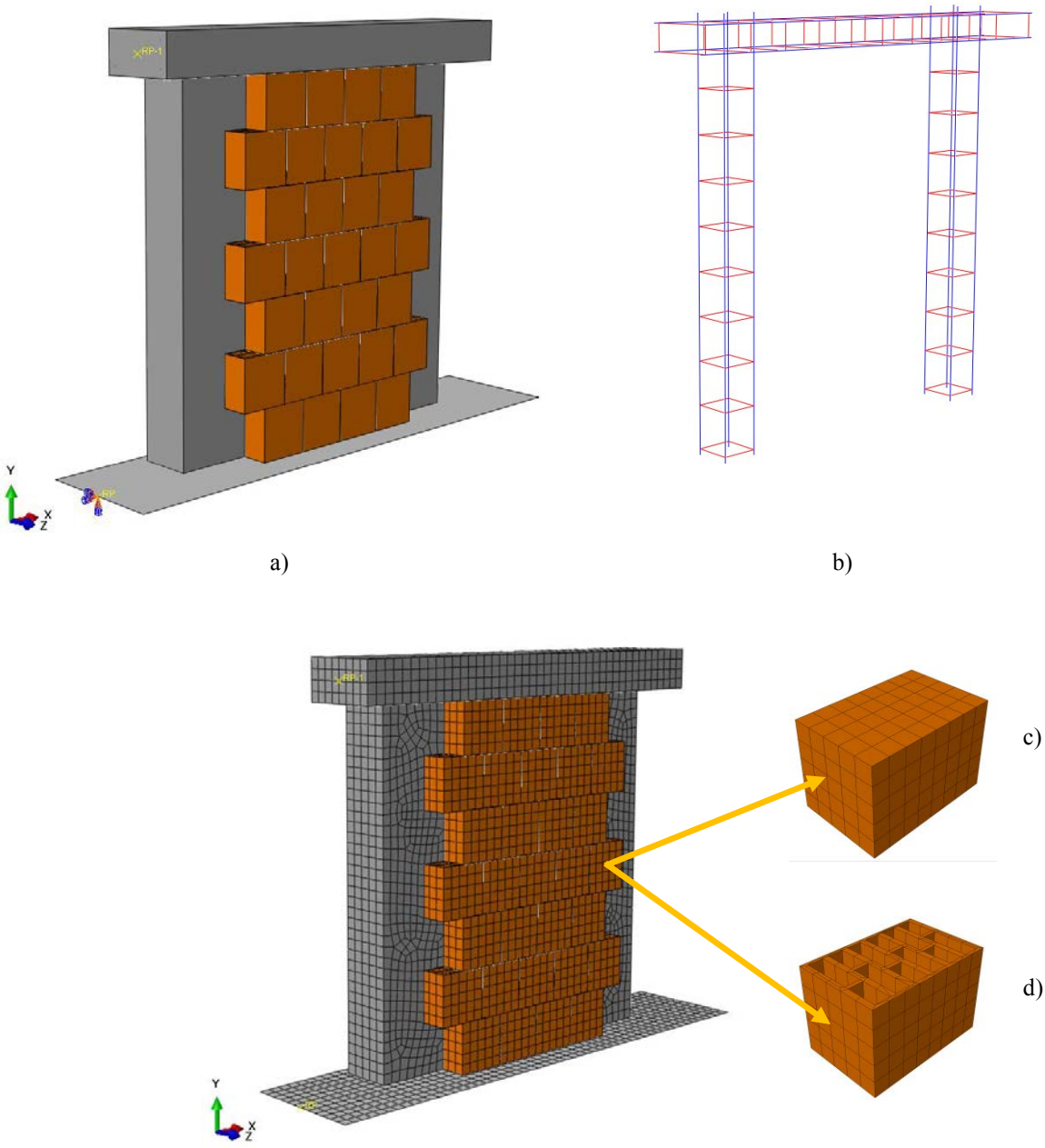

Figure 6: The numerical model built in Abaqus [16]: a) modelling of tie-columns, bond beam and masonry units; b) modelling of reinforcement; c) mesh of the FE model 1 with solid units; d) mesh of the FE model 2 with units with holes.

The contact interface between the units, both vertical and horizontal, as well as joints between the RC confining elements and masonry units have been defined using general contact with the specified interaction properties. Two interaction properties have been defined, with the first defined as a global property assignment to all elements that are in contact. For this type of interaction, “hard” contact for the normal direction and penalty friction formulation for the-

tangential direction with a frictional coefficient of 0.57 has been assigned. Since head joints were unfilled, global property assignment has been used for them.

The second interaction property was defined as individual contact property to represent bed-joint behaviour, and it was assigned to the horizontal surfaces of the blocks in contact. This interaction property, beside "hard" contact and penalty friction assignment, contains surface-based cohesive interaction. Surface-based cohesive behaviour of the contact interface is suitable for situations in which the interface thickness is negligibly small (PU glue in joints is described in subsection 2.1). The interaction between masonry blocks and RC surrounding confining elements is also modelled with the interaction property adopted to represent the bed-joint (individual contact).

The behaviour of the interface before damage is linear elastic with normal and shear stiffnesses calculated according to the equations proposed by Nazir and Dhanasekar [17]:

$$K_{nn} = \frac{E_u E_m}{E_u \left(h_u + h_j \right) - E_m h_u} \tag{1}$$

$$K_{ss} = K_{tt} = \frac{K_{nn}}{2\left(1+\nu\right)} \tag{2}$$

where E_u and E_m are modulus of elasticity of the unit and masonry, respectively. Height of unit is denoted as h_u and joint thickness as t_j.

Modulus of elasticity of the unit can be determined by multiplying the compressive strength of the unit by 300 according to [18]:

$$E_u = 300 f_{bk} \tag{3}$$

Table 1 presents an overview of values adopted for defining interaction properties for both numerical models used in this study. As described above, normal and shear stiffnesses that define the linear elastic behaviour of traction-separation model are calculated according to the recommendations given in [17]. The value for maximum tensile stress used as damage initiation criterion (t_n^0) is taken from [19]. Maximum shear stresses (t_s^0 and t_t^0) is taken from triplet experimental test. For damage evolution, values for fracture energies (G_n, G_s and G_t) are defined by trial and error in the calibration process. Friction coefficient, μ, was also taken from the experiment.

Interaction properties	Values used in FE model 1	Values used in FE model 2
K_{nn} [MPa/mm]	89.55***	12.193***
K_{ss} [MPa/mm]	37.31***	5.08***
K_{tt} [MPa/mm]	37.31***	5.08***
t_n [MPa]	0.19**	0.19**
t_s [MPa]	0.097*	0.097*
t_t [MPa]	0.097*	0.097*
G_n [N/mm]	0.001**	0.001**
G_s [N/mm]	0.02**	0.02**
G_t [N/mm]	0.02**	0.02**
η [-]	2**	2**
μ [-]	0.57*	0.57*
*The value is taken from the dedicated tests. **The value is calibrated. ***The value is calculated.		

Table 1: Material property values used for interactions for FE models 1 and 2.

3.2 Material models

3.2.1 Concrete

The nonlinear behaviour of concrete and masonry was modelled by the Concrete Damaged Plasticity (CDP) model. The CDP model assumes that the main two failure mechanisms are tensile cracking and compressive crushing of the concrete material. This constitutive model is designed to simulate the behaviour of concrete and other quasi-brittle materials subjected to monotonic as well as cyclic loading [16].

The plastic response of concrete requires the definition of stress-strain curves for compression and tension in combination with plasticity evolution parameters. The stress-strain relations under uniaxial tension and compression are defined as in the equations (4) and (5):

$$\sigma_t = (1-d_t)E_0(\varepsilon_t - \varepsilon_t^{pl}) \tag{4}$$

$$\sigma_c = (1-d_c)E_0(\varepsilon_c - \varepsilon_c^{pl}) \tag{5}$$

where E_0 is the initial (undamaged) elastic stiffness, ε_t and ε_c are the total tensile and compressive strains of the material, respsectively, while ε_t^{pl} and ε_c^{pl} are the respective corresponding equivalent plastic strains.

Under uniaxial compression, the stress-strain curve was determined according to the equations given in [20]. The tensile behaviour is defined using a fracture energy criterion and a stress-displacement curve instead of a stress-strain curve, as described in [21].

In order to fully define the behaviour of concrete under uniaxial compression and tension, it is also necessary to define the damage parameters. The degradation of the elastic stiffness is characterized by two damage variables, d_t and d_c, which are assumed to be functions of the inelastic strains [16]. Damage variables can take values from zero to one, representing the transition from undamaged to completely damaged material. The damage parameters are calculated using the following exponential equations (6) and (7), as proposed in [22]:

$$d_t = 1 - e^{-\alpha_t \varepsilon_t^{in}} \tag{6}$$

$$d_c = 1 - e^{-\alpha_c \varepsilon_c^{in}} \tag{7}$$

where α_t and α_c are damage evolution parameters for the uniaxial tension and compression, respectively. They are usually obtained by calibration with the experimental results.

Damage curves used in this study for concrete material under compression and tension are given in Figure 7.

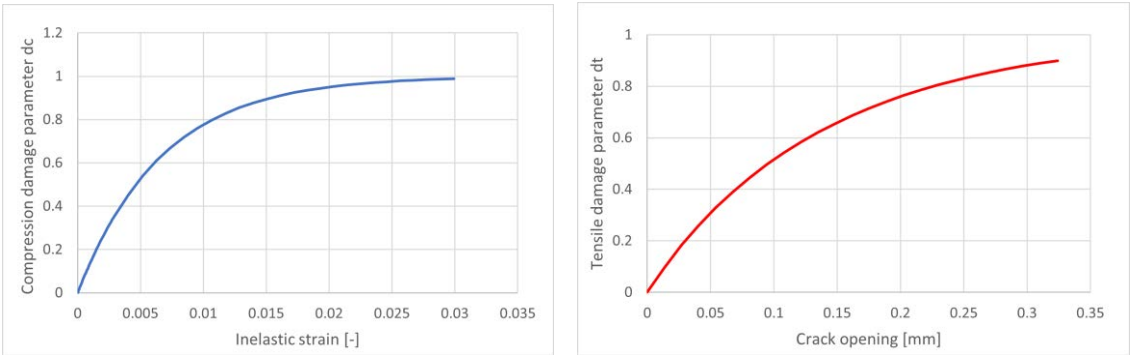

Figure 7: Damage curves for concrete in compression (left) and tension (right).

Material properties for reinforcing steel were based on the results of uniaxial tests of used reinforcement and are presented in Table 2, along with the material characteristics for the concrete model.

Concrete	Values used in FE models 1 and 2	Reinforcing steel	Values used in FE models 1 and 2
E_{cm} [MPa]	33 000*	E_s [MPa]	200 000****
f_{cm} [MPa]	38*	Poisson's ratio [-]	0.3***
$\varepsilon_{c,el}$ [‰]	0.495***	f_y [MPa]	551****
$f_{c,el}$ [MPa]	15.2***	f_u [MPa]	658****
$\varepsilon_{c,1}$ [‰]	2.2*	ε_u [%]	0.18****
k [-]	2.006***	*The value is taken from the Standard EC2. **The value is calibrated. ***The value is calculated. ****The value is taken from the dedicated tests.	
$\varepsilon_{c,uD}$ [‰]	3.5*		
$f_{c,uD}$ [MPa]	24.86***		
$\varepsilon_{c,uE}$ [‰]	3.0**		
α [-]	19**		
α_{tD} [-]	0.5**		
α_{tE} [-]	0.9**		
β [-]	1.529***		
f_{ctm} [MPa]	2.9*		
$\varepsilon_{t,el}$ [‰]	0.088***		
c_1 [-]	3.0**		
c_2 [-]	6.93**		
G_F [N/m]	183.0***		
U_c [mm]	0.324***		
α_c [-]	150**		
α_t [-]	350**		
l_{eq} [m]	0.05**		

Table 2: Material property values used for concrete and reinforcing steel for FE models 1 and 2.

3.2.2 Masonry units

The nonlinear model used for clay blocks is again the Concrete Damage Plasticity (CDP) model. The material parameters, however, are different and correspond to the behavior of clay blocks. A detailed description of the definition of the material model approach for masonry is used as described in [20]. The damage evolution curves for masonry units were generated in the same way as for concrete material and presented in Figure 8 for FE model 1. Damage curves used for FE model 2 are generated in the same way just using different ultimate strain.

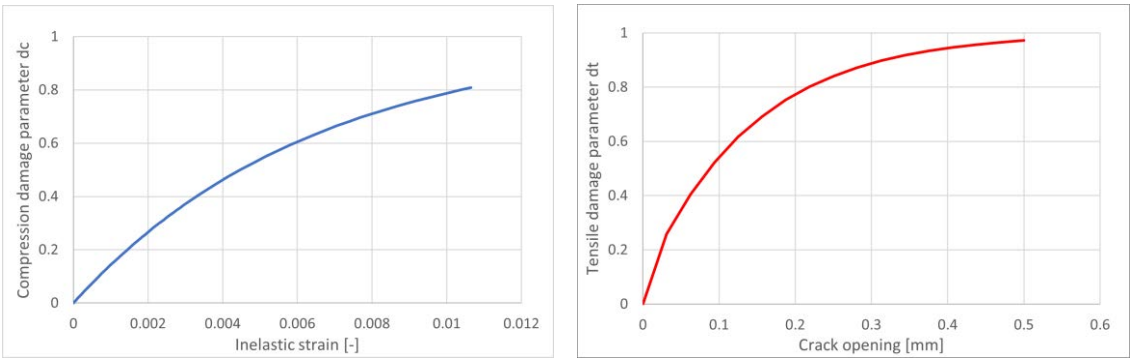

Figure 8: Damage curves for masonry units in compression (left) and tension (right) used in FE model 1.

The values of the material properties used for the clay blocks are summarized in Table 3 (for numerical models 1 and 2), where it can be seen which values were taken directly from the experiment, calculated according to the recommendation from the literature or calibrated.

Clay blocks	Values used in FE model 1	Clay blocks	Values used in FE model 2
E_m [MPa]	2200*	E_u [MPa]	7875*** (300 $f_{bk,neto}$)
f_m' [MPa]	3.8*	$f_{bk,bruto}$ [MPa]	10.5*
$\varepsilon_{m,el}$ [‰]	0.15**	$f_{bk,neto}$ [MPa]	26.25*** (f_{bk} / 0.4)
ε_1 [‰]	3.5**	$\varepsilon_{m,el}$ [‰]	0.65**
σ_D [MPa]	3.42**	ε_1 [‰]	6.5**
ε_2 [‰]	4.6**	σ_D [MPa]	23.64**
f_{mt}' [MPa]	0.38*** (10% f_m')	ε_2 [‰]	8.55**
$\varepsilon_{m,cr}$ [‰]	0.173**	f_{mt} [MPa]	1.313** (5% $f_{bk,neto}$)
r_t [-]	0.05**	$\varepsilon_{m,cr}$ [‰]	0.167**
α_1 [-]	300**	r_t [-]	0.05**
α_t [-]	460**	α_1 [-]	750**
l_{eq} [m]	0.05**	α_t [-]	380**
Poisson's ratio [-]	0.2***	l_{eq} [m]	0.05**
		Poisson's ratio [-]	0.2***
*The value is taken from the dedicated tests. **The value is calibrated. ***The value is calculated.			

Table 3: Material property values used for clay blocks in FE models 1 and 2.

3.3 Results of numerical simulations

In this subsection the results of numerical are be presented and, as mentioned earlier, compared with experimental results in terms of capacity curve, damage propagation and shear-off effect. In the experimental tests, the walls were tested under cyclic load, whereas in the numerical simulations, the load was applied in a monotonic manner (from left to right).

The capacity curves obtained from the experimental tests on two full-scale modern confined masonry (CM) walls and numerical simulations on two 3D FE models carried out in Abaqus [14] are shown in Figure 9.

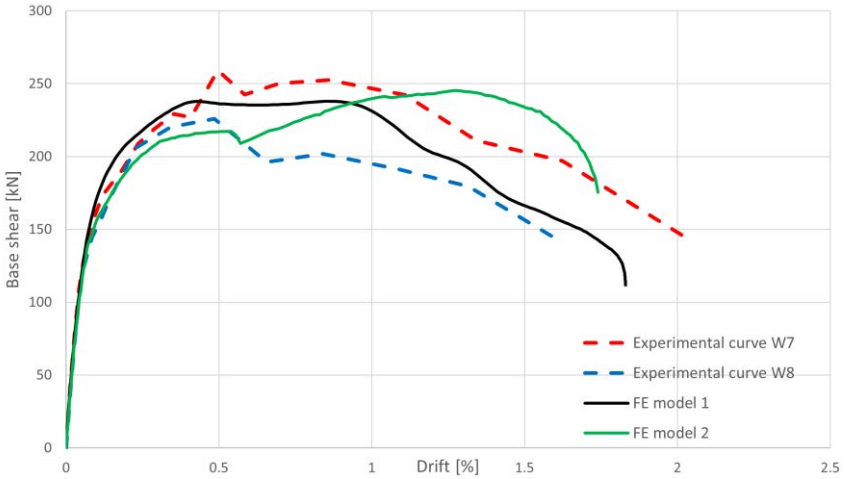

Figure 9: Comparison of the experimental and numerical force-drift curves.

The numerical curve obtained from FE model 1 (black) shows a quite good alignment with the experimental envelope curves (blue and red dashed) in terms of initial stiffness, peak load

capacity and stiffness degradation. The alignment is good especially if an average response curve of W7 an W8 is considered. This is further confirmed in Table 4, which numerically analyzes the difference in forces and drifts for considered limit states. The numerical and experimental curves (specimens W7 and W8) are very similar in these limit states, including in the Near Collapse LS.

The numerical curve obtained from FE model 2 (green), which uses the actual geometry of the blocks instead of full blocks, showed somewhat worse alignment of response curves. After a good aligmnemnt in the elastic phase, the numerical model curve's first peak is reached at a drift of about 0.53%. The experimental curves peaked at a drift of 0.54% and 0.49% for specimens W7 and W8, respectively. According to Table 4 (in simulation M2), the difference in forces when the maximum peak capacity is reached is about 15%, which means that the peak capacity is underestimated. After reaching the maximum capacity in FE model 2, the base shear force continues to increase with increasing drift, which was obviously not observed in the experiment. The second peak of the numerical curve is reached at a peak force of about 245 kN but at a significantly overestimated drift of about 1.3%.

	Damage LS		Max. Resist. LS		Near Collapse LS	
	F [kN]	Φ [%]	F [kN]	Φ [%]	F [kN]	Φ [%]
Experiment W7	162.7	0.09	259.0	0.54	128.8	2.03
Experiment W8	151.0	0.085	247.0	0.49	140.9	1.62
Simulation M1	160.14	0.083	237.94	0.48	113.78	1.83
Difference W7/M1 [%]	-1.57	-7.78	-8.13	-11.11	-11.66	-9.85
Difference W8/M1 [%]	+5.71	-2.35	-3.67	-2.04	-19.25	+11.48
Simulation M2	155.70	0.092	217.31	0.53	169.42	1.74
Difference W7/M2 [%]	-4.30	+2.17	-16.10	-1.85	+26.58	-14.29
Difference W8/M2 [%]	+3.02	+7.61	-12.02	-7.55	+19.68	-6.90

Table 4: Comparison of numerical and experimental results on confined masonry walls. Simulations M1 and M2 refer to FE models 1 and 2, respectively.

Figures 10 and 11 compare the experimental results and the results of numerical simulations (FE models 1 and 2) in terms of damage propagation and stress distribution at limit states. Figure 10a) shows the crack pattern on the tested wall specimen W8 at the Damage LS, when a lightly visible stepped diagonal crack developed through the wall. A similar propagation of diagonal struts can be noticed in the FE models 1 and 2, as shown in Figures 10b) and c). Like in the tested specimen W8, each diagonal strut's width equals approximately half of the clay block length.

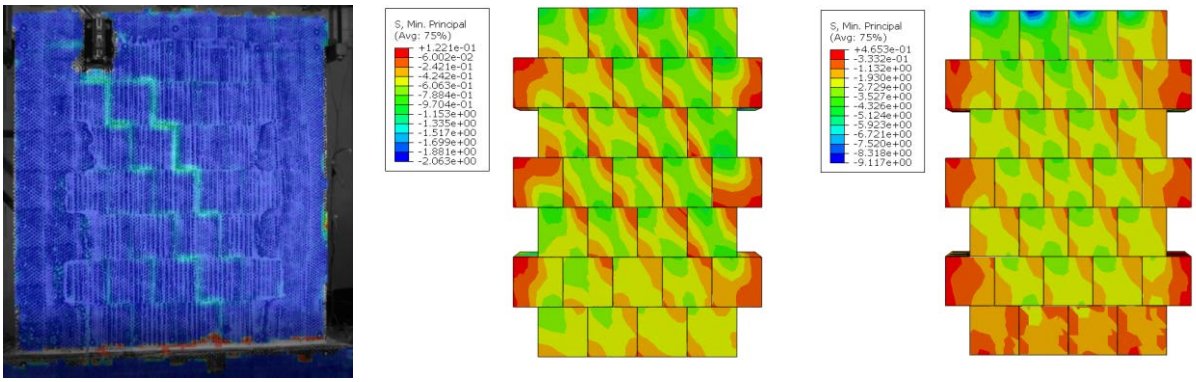

a) b) c)

Figure 10: a) Experimental crack pattern at drift corresponds to Damage LS; Distribution of minimum principal stresses from the b) FE model 1 and c) FE model 2.

During the transition from the first (Damage LS) to the second (Maximum resistance LS) limit state, the clay blocks on the non-fully confined side of the wall affect the local damage evolution, as the non-fully confined side begins to crack and damage along the shear plane. Despite this, the main damage of the wall specimen W8 is still a diagonal stepped crack that is clearly pronounced, as seen in Figure 11a). Regarding the numerical results from FE models 1 and 2 (see Figures 11b) and c)), a similar distribution of diagonal struts can be observed, as in the previous drift corresponding to the Damage LS.

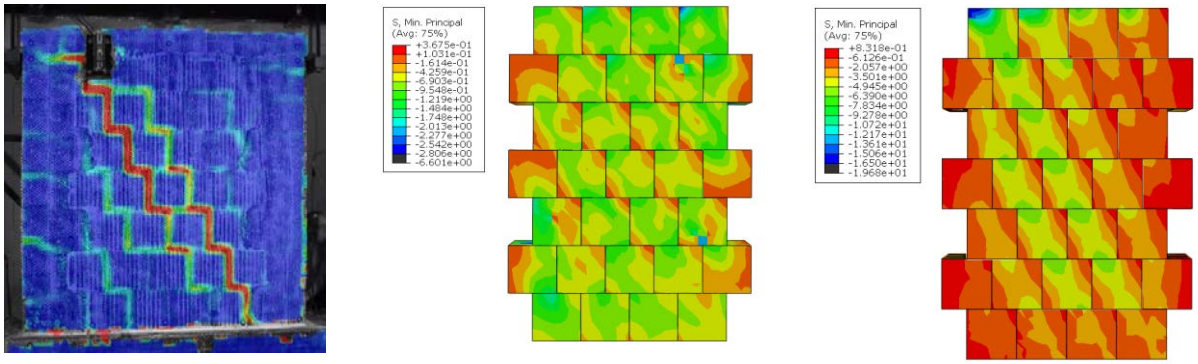

a) b) c)

Figure 11: a) The crack propagation at drift corresponds to Maximum Resistance LS; Distribution of minimum principal stresses from the b) FE model 1 and c) FE model 2.

Horizontal cracks in tie-columns appear along the entire height of the tie-column (see Figure 12a), which indicates tensile loads and damage in the tie-columns. During the experiments, the first cracks in concrete can be observed already at about 0.3 % drift. At a drift of about 0.5%, which corresponds to the Maximum resistance LS, in addition to horizontal cracks throughout the height of the tie-column, the damage in the tie-columns becomes concentrated in inclined (shear) cracks in the upper corner of the left tie-column and the lower corner of the right tie-column (Figure 12).

The failure mechanism can be better determined after the observation of stress distribution at different drift levels in both FE models. For instance, Figures 10 and 11 show the distribution of minimum principal stresses at different levels of drift, which indicates the appearance of compressive struts and formation of stepped cracks thorught the wall specimen. Also, it can be seen from Figure 12 that the crack spreads further and is transferred to the surrounding RC tie-columns, which causes shear failure in the modern CM wall.

It should also be noted that in FE model 1 blocks laid on diagonal struts suffer more damage and there are more tensile cracks in the clay blocks (Figure 12a). On the other hand, in FE model 2, the first visible cracks occur in the RC tie-columns, while the clay blocks remain practically undamaged (see Figure 12b) due to the high compressive and tensile strengths of the clay material.

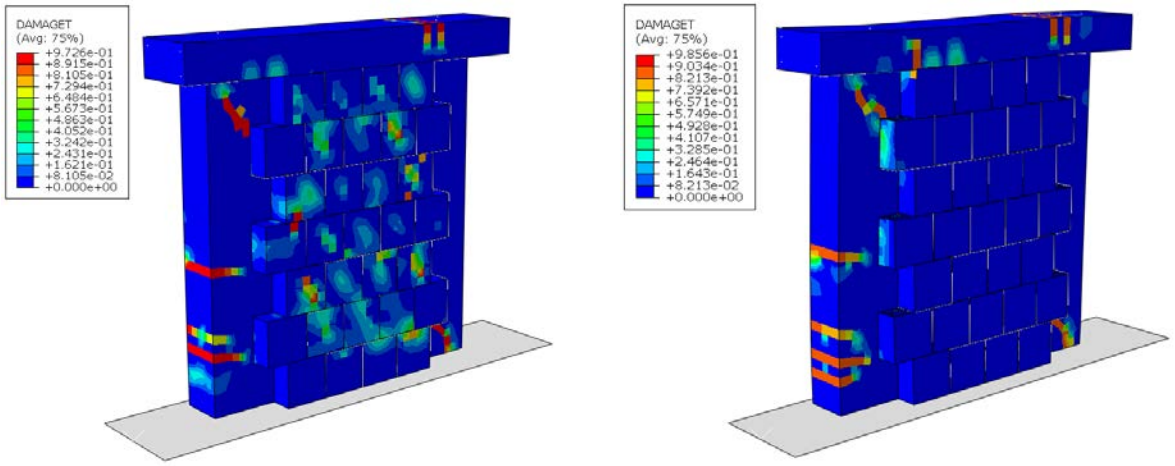

a) b)

Figure 12: Tension damage distribution at drift corresponds to Maximum Resistance LS in tension in a) FE model 1 and b) FE model 2.

As mentioned in Chapter 2, an interesting local effect was observed during the experimental tests. The difference in thickness of the wall and RC ties creates stress concentrations and damage to the protruding parts of the CM wall. This effect could successfully be modelled using FE model 2 with actual block geometry, as shown in Figure 13.

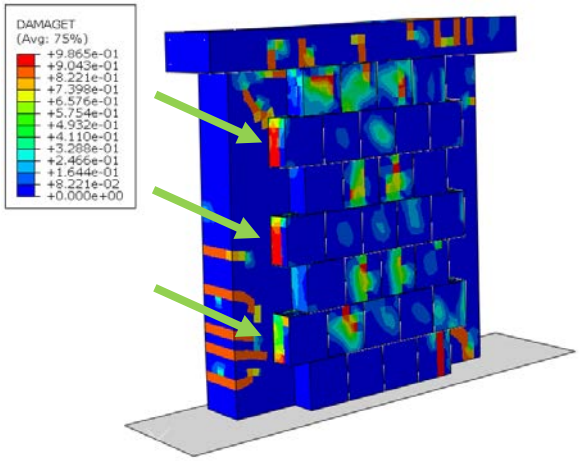

Figure 13: Numerical simulation of the shear-off effect of unconfined parts of clay blocks. Green arrows indicate shearing of protruding masonry.

4 CONCLUSIONS

This paper presents the results of experimental shear compression tests on two full-scale confined masonry walls built from hollow clay masonry blocks and PU glue. In the tests it was observed that because the walls are thick and tie-columns are narrower than the masonry, the protruding part of masonry shears off. The seismic response and the shearing phenomenon were modelled using detailed 3D FE models in Abaqus software. Two approaches to numerical modelling were employed. In the first one, the blocks were modelled as solid elements, whereas in the second, masonry blocks were modelled using their actual geometry.

The results of simulations have shown that:

(1) FE model 1, which uses models blocks as solid elements, replicates global response in terms of the capacity curve, damage propagation, and limit states very well. However, it is not capable of replicating the shearing off phenomenon.

(2) The more refined model (FE model 2), which models the actual geometry of the blocks, is less successful in replicating global response, especially in the post peak response. The shear-off effect, on the other hand, could be simulated.
(3) Results of numerical simulations show that the 3D detailed FE model developed in this work is able to replicate the behavior of modern CM walls in terms of capacity curve and damage evolution.
(4) The numerical simulations give new insight into the interaction between RC ties and masonry. Therefore, the recommended 3D FE models should be verified and improved by additional experiments and additional numerical simulations in the future.

ACKNOWLEDGMENTS

The research presented in this paper was sponsored by the Slovenian Research Agency (program P2-0185). This support is gratefully acknowledged.

REFERENCES

[1] S. Brzev, K. Mitra, *Earthquake-resistant confined masonry construction, 3th Edition*. Uttar Pradesh, India: NICEE, National Information Center of Earthquake Engineering, Indian Institute of Technology Kanpur, 2018.

[2] R. Meli, S. Brzev, M. Astroza, T. Boen, F. Crisafulli, J. Dai, M. Farsi, T. Hart, A. Mebarki, A.S. Moghadam, D. Quiun, M. Tomaževič, and L. Yamin. Seismic Design Guide for Low-Rise Confined Masonry Buildings. Confined Masonry Network, Earthquake Engineering Research Institute, Oakland, CA, USA, 2011 (available free of charge at www. confinedmasonry.org).

[3] M. Astroza, O. Moroni, S. Brzev, J. Tanner, Seismic Performance of Engineered Masonry Buildings in the 2010 Maule Earthquake. *Special Issue on the 2010 Chile Earthquake, Earthquake Spectra*, **28** (S1), S385-S406, 2012.

[4] S. Brzev, M. Astroza, O. Moroni, Performance of confined masonry buildings in the February 27, 2010 Chile earthquake. California, Oakland, Earthquake Engineering Research Institute, 2010.

[5] E. Miranda, S. Brzev, N. Bijelić, Ž. Arbanas, M. Bartolac, V. Jagodnik, D. Lazarević, et al., StEER-EERI: Petrinja, Croatia December 29, 2020, Mw 6.4 Earthquake Joint Reconnaissance Report (JRR). The Structural Extreme Events Reconnaissance (StEER) Network, United States, 2021.

[6] J. Varela-Rivera, L. Fernandez-Baqueiro, J. Gamboa-Villegas, A. Prieto-Coyoc, J. Moreno-Herrera, Flexural behavior of confined masonry walls subjected to in-plane lateral loads. *Earthquake Spectra*, **35** (1): 405–22, 2019. https://doi.org/10.1193/112017EQS239M

[7] R. Marques, P.B. Lourenço, Structural behaviour and design rules of confined masonry walls: Review and proposals. *Construction and Building Materials*, **217**, 137–55, 2019. https://doi.org/10.1016/j.conbuildmat.2019.04.266

[8] V. Singhal, D.C. Rai, In-plane and out-of-plane behavior of confined masonry walls for various toothing and openings details and prediction of their strength and stiffness. *Earthq. Eng. Struct. Dyn*, **45** (15): 2551-2569, 2016. doi: https://doi.org/10.1002/eqe.2783

[9] B. Borah, V. Singhal, H.B. Kaushik, Assessment of seismic design provisions for confined masonry using experimental and numerical approaches. *Engineering Structures*, **245**, 112864, 2021. https://doi.org/10.1016/j.engstruct.2021.112864

[10] B. Borah, H.B. Kaushik, V. Singhal, Finite Element Modelling of Confined Masonry Wall under In-plane Cyclic Load. *International Conference on Materials, Mechanics and Structures (ICMMS2020)*, Kerala, India, July 14-15, 2020. doi:10.1088/1757-899X/936/1/012020

[11] H. Okail, A. Abdelrahman, A. Abdelkhalik, M. Metwaly, Experimental and analytical investigation of the lateral load response of confined masonry walls. *HBRC Journal*, **12** (1), 33-46, 2016. doi: 10.1016/j.hbrcj.2014.09.004

[12] R. Marques, J.M. Pereira, P.B. Lourenço, Lateral in-plane seismic response of confined masonry walls: from numerical to backbone models. *Engineering Structures*, **221**, 111098, 2020. doi: https://doi.org/10.1016/j.engstruct.2020.111098

[13] P.B. Lourenço, Computational Strategies for masonry Structures. Dissertation, Faculty of Civil Engineering and Geosciences, TU Delft, The Netherlands, 1996.

[14] Dassault, Abaqus/Explicit FEA. Dassault Systèmes Simulia Corporation, 2023.

[15] N. Krtinić, M. Gams, M. Marinković, Pushover analysis of confined masonry walls using equivalent diagonal strut models. In *Proceedings of the 2th Croatian Conference on Earthquake Engineering (2CroCEE),* Zagreb, Croatia, March 22-24, 2023.

[16] Dassault, Abaqus 6.14. User's Manual, Dassault Systèmes Simulia Corporation, 2014.

[17] S. Nazir, M. Dhanasekar, A non-linear interface element model for thin layer high adhesive mortared masonry. *Computers and Structures*, **144**, 23-39, 2014. doi: https://doi.org/10.1016/j.compstruc.2014.07.023

[18] H. B. Kaushik, D.C. Rai, S. K. Jain, Stress-strain characteristics of clay brick masonry under uniaxial compression. *Journal of Materials in Civil Engineering*, **19** (9), 728–739, 2007. doi: 10.1061/(ASCE)0899-1561(2007)19:9(728)

[19] M. Marinković, Innovative system for seismic resistant masonry infills in reinforced concrete frame structures. Dissertation, Faculty of Civil Engineering, University of Belgrade, Serbia, 2018.

[20] M. Marinković, C. Butenweg, Numerical analysis of the in-plane behaviour of decoupled masonry infilled RC frames. *Engineering Structures*, **272**, 114959, 2022. doi: https://doi.org/10.1016/j.engstruct.2022.114959

[21] T. Kubalski, C. Butenweg, M. Marinković, S. Klinkel, Investigation of the seismic behaviour of infill masonry using numerical modelling approaches. In *Proceedings of the 16th World Conference on Earthquake Engineering (16WCEE 2017),* Santiago, Chile, January 9-13, 2017.

[22] J. Lee, G. L. Fenves, Plastic-damage model for cyclic loading of concrete structures. *Journal of Engineering Mechanics*, **124** (8), 892-900, 1998.